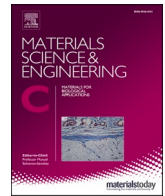




Contents lists available at ScienceDirect

Materials Science & Engineering C

journal homepage: www.elsevier.com/locate/msec

Micro-arc oxidation-assisted sol-gel preparation of calcium metaphosphate coatings on magnesium alloys for bone repair

Yanping Liu^{a,1}, Xian Cheng^{b,c,1}, Xiyuan Wang^d, Qiu Sun^d, Chenxi Wang^a, Ping Di^{a,*}, Ye Lin^{a,*}

^a Department of Oral Implantology, Peking University School and Hospital of Stomatology, Beijing 100081, China

^b Xiangya Hospital Stomatological Hospital, Central South University, Changsha, Hunan 410000, China

^c Department of Dentistry-Biomaterials, Radboud University Medical Center, Philips van Leydenlaan 25, 6525 EX Nijmegen, the Netherlands

^d School of Chemistry and Chemical Engineering, Harbin Institute of Technology, Harbin 150001, China

ARTICLE INFO

Keywords:

Calcium metaphosphate
Magnesium alloy
Micro-arc oxidation
Sol-gel
Corrosion resistance
Bone repair

ABSTRACT

Calcium phosphate coating is an attractive surface modification strategy for magnesium alloys, since it can increase their corrosion resistance and endow them with osteogenic function simultaneously. Herein, a calcium metaphosphate (CMP) coating was fabricated on magnesium alloy by using sol-gel approach assisted with micro-arc oxidation pre-treatment. Scanning electron microscopy showed that the micro-pores and cracks in micro-arc oxidation inner layer generated during the pre-treatment process were sealed by the grainy sol-gel outer layer. Energy dispersive spectrometry and X-ray diffraction results demonstrated the identity of the coating as CMP. The cross-cut test showed that the adhesion of CMP coating was strong. Applying bare magnesium alloy substrate as a control, the CMP coating surface was rougher and more hydrophilic. The potentiodynamic polarization test demonstrated that the corrosion resistance was significantly improved by using CMP coating. Hydrogen evolution in immersion test further confirmed that the degradation rate was decelerated within 14 days. Moreover, CMP coating facilitated the adhesion speed, spreading area, and focal adhesion formation of bone marrow stem cells. The number of cells in the active proliferating state and proliferated cells present on the CMP coating also increased. Additionally, CMP coating upregulated alkaline phosphatase activity and osteogenic gene expression in cells. In summary, the micro-arc oxidation assisted sol-gel CMP coatings increased the corrosion resistance and promoted the interfacial cell behavior for magnesium alloy implants, which might inform the further development of surface modifications on magnesium alloys for bone related applications.

1. Introduction

Magnesium (Mg) alloys have attracted widespread attention on bone repairing due to their degradability and excellent mechanical properties [1]. However, there are still some challenges associated with using Mg alloys as scaffold or implants for bone related applications [1–3]. First, the degradation rate of Mg alloys is too fast that the supportive function is often lost before bone tissue healing is completed [4]. Furthermore, the hydrogen and hydroxyl ions produced during Mg alloy degradation lead to emphysema and a high pH microenvironments near the Mg alloys, respectively, which influences osteoblastic growth and bone regeneration [5,6]. Moreover, Mg alloys are lack of bioactivity and osteoconductivity [4,7,8]. Therefore, calcium phosphate based coating

system is a promising surface modification strategy for Mg alloys, since it can improve their corrosion resistance and endow them with osteogenic function simultaneously [2,9].

Among different calcium phosphates, calcium metaphosphate (CMP; $\text{Ca}(\text{PO}_3)_2$) is a promising bone substitute material due to its desirable osteoconductive and biodegradable properties [10]. *In vitro* and *in vivo* studies revealed that CMP is beneficial to the osteoblastic differentiation and can provoke specific biological responses at the interface of the materials and bone tissue, resulting in the formation of a strong bond [10,11]. Moreover, the degradation rate of CMP consistently occurs along with the growth of bone tissue [13]. Despite these advantages that indicate CMP as a suitable coating material for Mg alloys, neither its preparation nor its physicochemical and biological characteristics have

* Corresponding authors at: Department of Oral Implantology, Peking University School and Hospital of Stomatology, 22 South Zhongguancun Avenue, Haidian District, Beijing 100081, China.

E-mail addresses: diping@bjmu.edu.cn (P. Di), yorcklin@263.net (Y. Lin).

¹ These authors contributed equally.

<https://doi.org/10.1016/j.msec.2021.112491>

Received 23 July 2020; Received in revised form 7 October 2021; Accepted 10 October 2021

Available online 14 October 2021

0928-4931/© 2021 Published by Elsevier B.V.

been reported.

Calcium phosphate coatings can be fabricated on Mg alloy substrates by various techniques [14,15]. Among these methods, sol-gel synthesis of calcium phosphate coatings by using dipping and spinning processes has attracted much research attention [16]. Based on mixing calcium and phosphorus precursors, this versatile approach can be applied to construct homogeneous calcium phosphate coatings with high purity and fine-tunable thickness on metallic substrates with several advantages including easy control of the chemical composition and microstructure, adaptability to coat substrates of complex shapes, high preparation efficiency, as well as upscaling potential for commercial production [16,17]. Unfortunately, a poor adhesion of the sol-gel calcium phosphate coating to substrate is a common disadvantage [18]. Moreover, for Mg alloy, the substrate corrosion may occur during the coating procedure itself [19], and the released Mg ion can compromise the crystallization process of the calcium phosphate coating [20,21].

Therefore, surface pre-treatments for the Mg alloy substrates, such as hydrothermal procedure, immersion in hydrofluoric acid, as well as micro-arc oxidation (MAO), is often required for making coatings on Mg alloys [22,23]. In all kinds of pre-treatments, MAO is recognized as an effective technology to produce a layer of magnesium oxide (MgO) on the Mg alloy surfaces [22,23]. This layer can serve as a transition layer to enhance the adhesion strength of post-prepared coatings, because the porous topography formed by MAO largely increase the contact area between coatings and substrates [24,25]. Furthermore, it can act as a physical protective layer to ensure the crystallization process of calcium phosphates during coating preparation [26]. The MAO layer also reduces the Mg alloy degradation rate by blocking the corrosive media to directly contact the Mg alloy substrates [26].

This study aimed to develop a CMP coating on Mg alloys by using sol-gel approach assisted with MAO pre-treatment for the dual purpose of delaying Mg alloy degradation rate and improving the osteogenic response of human bone marrow stem cells (hBMSCs). The surface features of the coatings were characterized using scanning electron microscopy, energy dispersive spectroscopy, and X-ray diffraction. The corrosion resistances were evaluated using potentiodynamic polarization and immersion tests. Additionally, hBMSCs were cultured on CMP coated Mg alloy and bare Mg alloy substrate. The osteogenic behavior of hBMSCs was investigated in terms of cell adhesion, spreading, proliferation, and osteogenic differentiation.

2. Materials and methods

2.1. Surface preparation

Commercial bare AZ31B Mg alloy was cut into disks, each with a diameter of 15 mm and a thickness of 2 mm. The disks were polished with silicon carbide papers and washed ultrasonically in acetone, ethyl alcohol, and deionized water for 10 min. The electrolytic polishing solution contained 8 g/L NaSiO₃, 5 g/L NaOH, and 1 g/L NaF. In a stainless-steel container equipped with a cooling system and a bi-directional pulse power supply, MAO was performed for 15 min at a current density of 20 A/dm², frequency of 300 Hz, and duty cycle of 15%. After the MAO process, the disks were washed in deionized water and then dried in air.

Sol-gel treatment was used to accomplish CMP coating on top of the MAO pre-treated coating. Ca(NO₃)₂·4H₂O and P₂O₅ were each dissolved in separate ethyl alcohol and agitated magnetically for 30 min. The two solutions were then mixed with the Ca/P molar ratio of 0.5 and stirred for 60 min to form the sol gel. The prepared sol-gel solution was spun onto the MAO pre-treatment disks with a rotation speed of 3000 rpm for 20 s. Then, the disks were preheated so that the film entered the amorphous phase. The procedure from spinning to preheating was repeated ten times. CMP in the amorphous phase was completely crystallized into a crystalline-phase film by a rapid annealing process, which involved heating to 600 °C in 6 s, maintaining at 600 °C for 180 s, and

cooling down to 30 °C in 30 s.

2.2. Surface characterization

The surface and cross-sectional morphologies of bare Mg alloy substrate, only MAO pre-treated Mg alloy, and CMP-coated Mg alloy were characterized using scanning electron microscope (Hitachi-S3400 N, Hitachi, Japan). The elemental composition analysis of the coatings was performed using linear energy dispersive spectrometer (IXRF-550i, Austin, TX, USA). X-ray diffraction studies of the samples were performed with a 2θ range of 20–70° using a diffractometer (D8, Bruker, Karlsruhe, Germany).

The universal surface tester (Innowep GmbH, Würzburg, Germany) was used to measure the thickness of coatings. The contact angles of deionized water on the surfaces of the samples were measured using a contact angle meter (CAST 3, KINO Co., Ltd., Boston, MA, USA). The surface roughness of the samples was measured with a 3D surface profiler (ContourGT-K0, Bruker, Karlsruhe, Germany). The adhesion quality of CMP coating and MAO pre-treated layer was ranked by different number from 0 to 5 in a cross-cut test (ISO-2409-1992). Briefly, a single-blade cutter was used to cut the coating lattice graphics and the adhesion level was determined according to the classification given in the standard. Grade 0 represents the best adhesion quality and no coating peeled off the substrate at all. Grade 5 represents the worst adhesion result with more than 65% of the area of the coating partially or completely peeled off. A stereo microscope (M205 C, Leica, Germany) was applied to identify the possible scratch clearly.

2.3. Electrochemical test

Corrosion resistances of bare Mg alloy substrate, MAO pre-treated Mg alloy, and CMP-coated Mg alloy were investigated through a potentiodynamic polarization test in simulated body fluid. The process was conducted in a conventional three-electrode electrochemical cell, with the saturated calomel electrode as the reference electrode, the graphite rod as the counter electrode, the test area of 1 cm² as the working electrode. The samples were soaked in the simulated body fluid solution for 30 min to ensure that the open circuit potentials were stabilized before the electrochemical measurements were made. The electrochemical test was carried out with a scanning speed of 1 mV per second at 37 °C. According to the Tafel extrapolation, the corrosion potential (E_{corr}) and corrosion current density (i_{corr}) were evaluated.

2.4. Immersion test

The immersion test was carried out in simulated body fluid according to ASTM-G31-72 [27]. The pH value was adjusted to 7.4 ± 0.1 and the temperature was kept at 37 ± 0.5 °C using a water bath. During the immersion test, the hydrogen evolution volumes were monitored for 14 days. After immersion for 14 days, the corrosion morphologies of the samples were presented by digital camera and scanning electron microscope.

2.5. Cell experiments

2.5.1. Cell culture

hBMSCs were purchased from Cyagen (Santa Clara, CA, USA). hBMSCs were cultured in α-modified Eagle's medium (α-MEM, Gibco, Waltham, MA, USA) supplemented with 10% fetal bovine serum (Gibco) and 1% penicillin/streptomycin. The cells were incubated at 5% CO₂ and 37 °C in a humidified atmosphere. After the hBMSCs reached 70–90% confluence, they were passaged using 0.25% trypsin and expanded until passages 4–6 for subsequent experiments. The prepared disks were sterilized by UV light and placed in 24-well plates. hBMSCs were seeded onto the surface of bare Mg alloy substrate and CMP-coated Mg alloy for obtaining 10,000 cells per well. The medium was changed

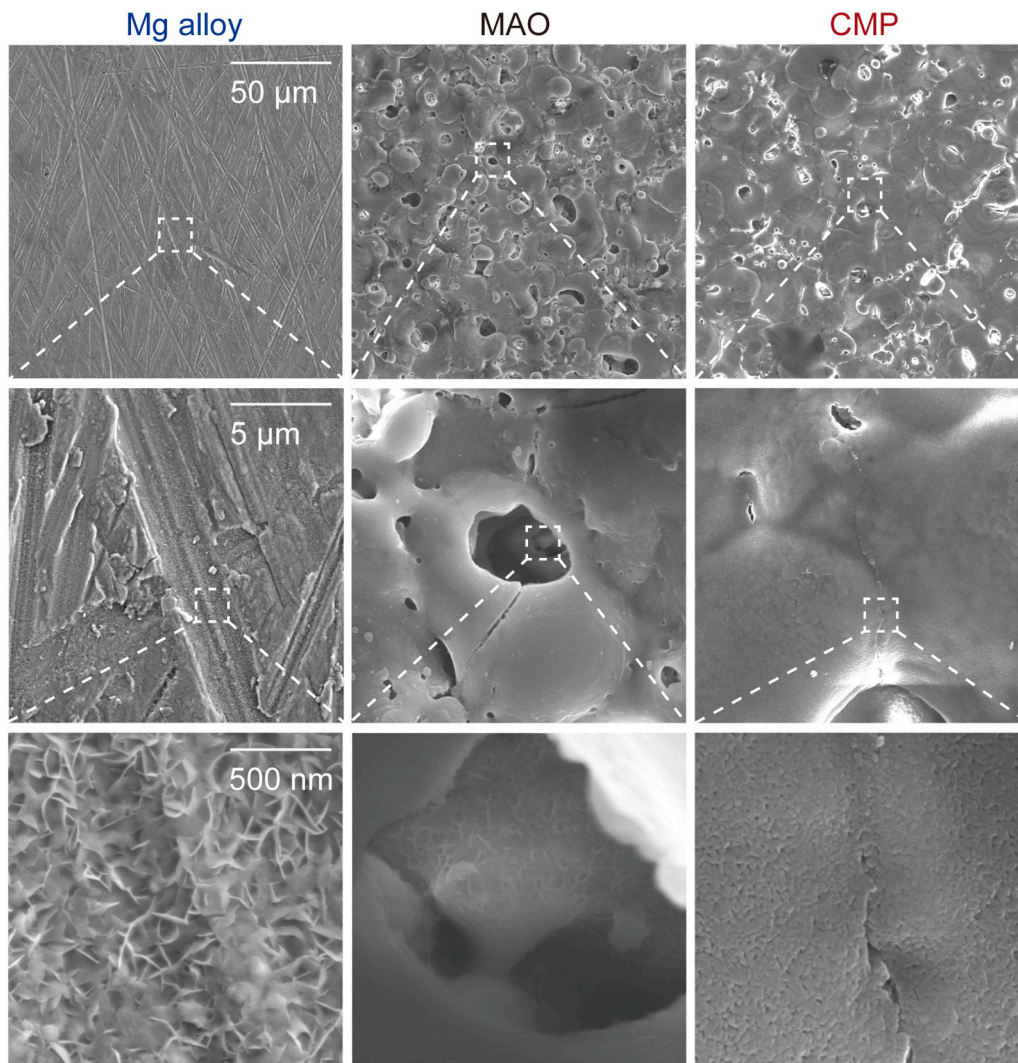


Fig. 1. Surfaces morphology observed by scanning electron microscope.

every 2–3 days.

2.5.2. Immunofluorescence

Cell adhesion was observed by immunofluorescence after cultivation for 1 h and 6 h, while cell spreading and proliferating state were observed after 24 h. The cells were fixed using 4% paraformaldehyde for 10 min, permeabilized with 0.1% Triton-X 100 for 10 min and washed three times in phosphate-buffered saline. The cells were incubated with 1% bull serum albumin for 1 h to block unspecific binding of the antibodies.

To stain the focal adhesions, samples were incubated with anti-vinculin primary antibody (1:400, ab129002, Abcam, U.S.A.) at 4 °C overnight, followed by incubation with Alexa-Fluor 647-conjugated secondary antibody (1:400, ab150083, Abcam, U.S.A.) at room temperature for 1 h. To label the F-actin, samples were incubated with TRITC-phalloidin (1:1000, P1951, Sigma, U.S.A.) for 30 min. Nuclei were counter stained using Vectashield Mounting Medium (Vector Labs, Burlingame, CA, USA) containing 40,6-diamidino-2-phenylindole (DAPI) for 5 min. Fluorescence images were captured using a light microscope (Olympus BX51, Olympus Co., Tokyo, Japan). Images analysis was performed by Image J (NIH, USA). To measure the cell adhesion stage and cell adhesion number, three random fields for each sample and three samples were analyzed per group. The quantitative measurement of focal adhesion area per cell followed a step-by-step protocol [28]. Image J was used to trace the cell borders to quantify the cell spreading

area. At least 30 cells were analyzed per group.

Similarly, to stain Ki-67, samples first were incubated with anti-Ki67 antibody (1:400, ab16667, Abcam, U.S. A.) and followed with Alexa-Fluor 594-conjugated secondary antibody (1:500, A32740, Abcam, U. S.A.). Nuclei were counter stained using DAPI for 5 min. The positive Ki-67 cell % was calculated based on the images taken from three random fields for each sample and three samples were analyzed per group.

2.5.3. Cell proliferation

After culturing for 24 h, 48 h, and 72 h, cell proliferation (three samples per group) was investigated using the Cell Counting Kit-8 assay. The wells with hBMSCs were rinsed with phosphate-buffered saline. The growth medium (500 μL) and Cell Counting Kit-8 solution (50 μL) were mixed and added to each well. Subsequently, the wells were incubated at 37 °C for 2 h, and the absorbance of the culture supernatants was measured at 450 nm.

2.5.4. ALP activity and osteoblast-related gene expression

Alkaline phosphatase (ALP) activity was determined using a staining kit (CoWin Biotech, Beijing, China) with nitro blue tetrazolium and 5-bromo-4-chloro-3-indolyl phosphate to evaluate the osteogenic differentiation of hBMSCs. Cells were cultured in growth medium and incubated for 7 days with medium change every 2–3 days. The cells were fixed in 4% paraformaldehyde for 10 min and rinsed in phosphate-buffered saline. Afterwards, ALP staining was carried out according to

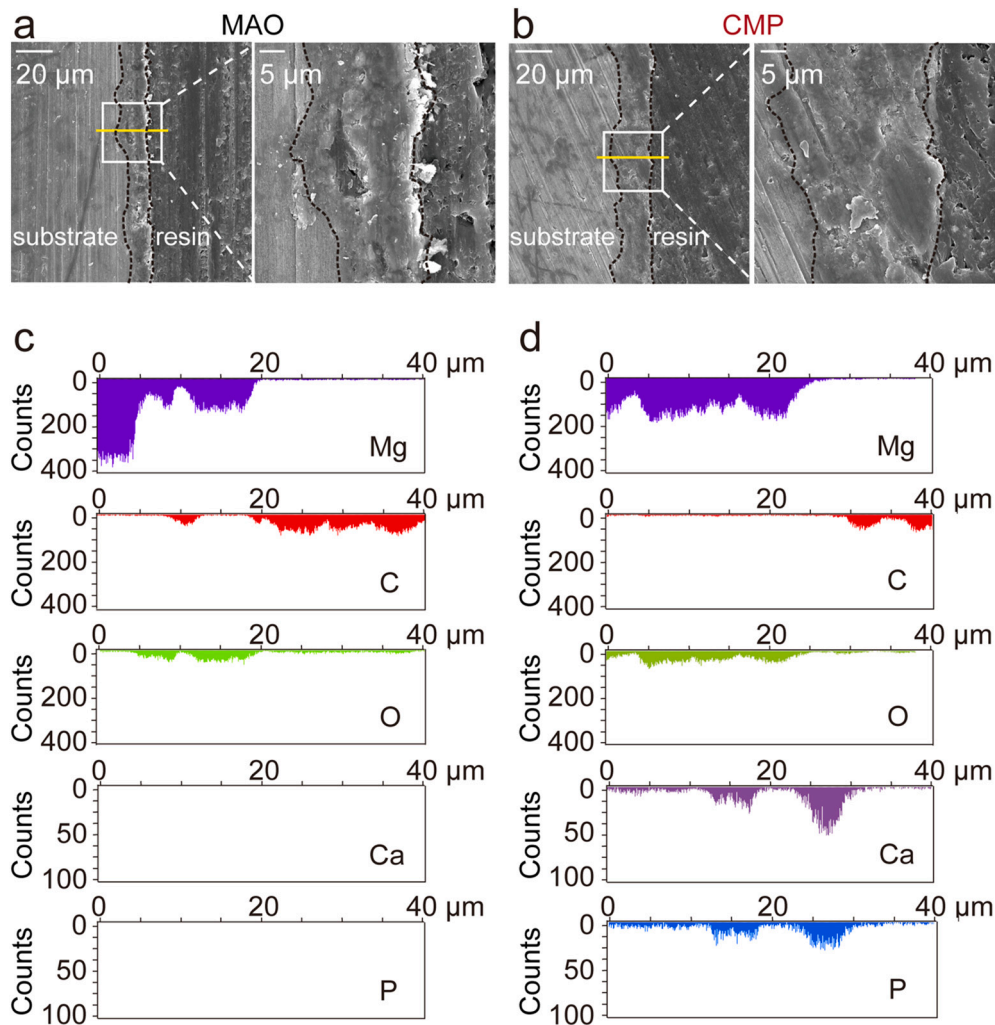


Fig. 2. Cross-sectional morphology and elementary analysis. The cross-sectional images of (a) only MAO pre-treated Mg alloys and (b) CMP coated Mg alloys observed by scanning electron microscope. Elemental distribution at a varying distance by energy dispersive spectrometer line scan (yellow line) of (c) only MAO pre-treated and (d) CMP coated Mg alloys. (For interpretation of the references to color in this figure legend, the reader is referred to the web version of this article.)

the manufacturer's instructions.

After cultivation for 7 days, total RNA extraction (three samples per group) was performed using the TRIzol reagent (Invitrogen, Carlsbad, CA, USA). RNA was reverse-transcribed into cDNA using a Reverse Transcription Kit (Takara, Kusatsu, Japan). Quantitative real-time polymerase chain reaction (qRT-PCR) was conducted to determine the transcript levels of *ALP*, runt-related transcription factor 2 (*RUNX2*), and type I collagen (*COL1*) using Power SYBR Green PCR Master Mix and an ABI PRISM 7500 sequence detection system (BGI, Shenzhen, China). Glyceraldehyde-3-phosphate (*GAPDH*) was used as the internal control. The primers used were *GAPDH*, (forward) 5'-AAC TTT GGC ATT GTG GAA GG-3' and (reverse) 5'-ACA CAT TGG GGG TAG GAA CA-3'; *ALP*, (forward) 5'-TTT GCT ACC TGC CTC ACT TCC G-3' and (reverse) 5'-GGC TGT GAC TAT GGG ACC CAG-3'; *RUNX2*, (forward) 5'-AAC AGC AGC AGC AGC AGC AG-3' and (reverse) 5'-GCA CCG AGC ACA GGA AGT TGG-3'; and *COL1*, (forward) 5'-CGT GAC CAA AAA CCA AAA GTG C-3' and (reverse) 5'-GGG GTG GAG AAA GGA ACA GAA A-3'. The cycle threshold values (Ct values) were used to calculate fold differences using the $2^{-\Delta\Delta Ct}$ method.

2.6. Statistical methods

The statistical analyses were performed using the Prism 7 software (GraphPad Software, San Diego, CA, USA). Statistically significant

differences were calculated by Student's *t*-test and ANOVA at $p < 0.05$. The data are expressed as mean \pm standard deviation.

3. Results and discussion

3.1. Material characterization

The surface morphologies of Mg alloy substrate, MAO pre-treated Mg alloy, and CMP coated Mg alloy are displayed in Fig. 1. The surface of the bare Mg alloy substrate exhibited grinding trace under low-magnification scanning electron microscopic image and scaly structures under high-magnification scanning electron microscopic image. With a MAO pre-treatment, a typical randomly porous microstructure with some cracks was observed on the surfaces, which is consistent with previous studies [29]. Some scaly structures could be seen on deeply porous surface regions, suggesting that some of the Mg alloy remained uncoated [30]. After CMP sol-gel coating was finally prepared, nanometer-sized CMP grains were distributed uniformly across the MAO surface where the micro-pores and cracks were sealed by the grains of the CMP coating.

The cross-sectional scanning electron microscopic images of MAO pre-treatment and CMP coating were displayed in Fig. 2a and b. The elemental distribution at a varying distance from substrate to the coating surfaces was explored by liner energy dispersive spectrometer. The

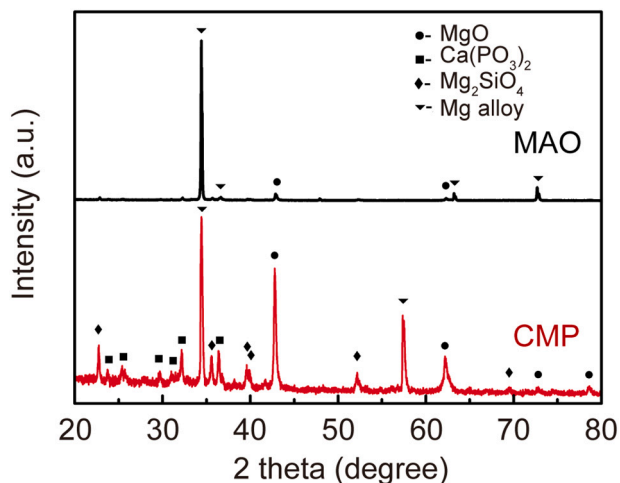


Fig. 3. Chemical composition analyzed by X-ray diffraction.

energy dispersive spectrometer analysis results demonstrated that the MAO pre-treated layer only included Mg and O (Fig. 2c), while Ca and P were present in the coating after the CMP sol-gel coating formation (Fig. 2d). It should be noted that two different peaks of Ca and P could be seen on the energy dispersive spectrometer spectra. One peak began to rise just out of the range of MgO layer, demonstrating that calcium phosphate coating covered the MAO surface. The other peak occurred inside the range of MgO layer. This peak may result from the fact that micro-pores and cracks inside the MgO layer were sealed by the calcium phosphate coating, which agreed with the scanning electron microscopic image results discussed above (Fig. 1).

X-ray diffraction patterns of the MAO pre-treated and CMP-coated surfaces are shown in Fig. 3. In the MAO pre-treated surface X-ray diffraction pattern, only the characteristic peaks of Mg and MgO were observed. After MAO and sol-gel treatment, the peaks of $\text{Ca}(\text{PO}_3)_2$ in the X-ray diffraction spectrum occurred, indicating the formation of crystallized CMP in the coating. The CMP sol-gel coating formation includes several stages: (i) formation of colloidal solution by hydrolysis and partial condensation of the precursors, (ii) formation of gel material with three-dimensional network by condensation of the sol particles, (iii) aging, and (iv) drying [31,32]. Upon aging, the hydrolyzed phosphorus sol (in the form of $\text{P}(\text{OH})_x(\text{OEt})_{5-x}$) interacted with calcium sol (in the form of $\text{Ca}(\text{NO}_3)_{2-y}(\text{OEt})_y$) in anhydrous ethanol to form oligomeric derivatives containing Ca–O–P bonds [15,31,32]. Further heating could remove the solvents, accompanied by accelerated thermal dehydration or polymerization/condensation between these derivative units, resulting in the formation of more (–Ca–O–P–) containing bonds in dry gels. [32]. Consequently, this amorphous calcium phosphate spun on the surface of MAO pre-treated Mg alloy converted to CMP after heating treatment at 600 °C, which coincides the previous study [15].

The Ra values (arithmetic averages of the roughness profile) for bare Mg alloy, MAO pre-treated Mg alloy, and CMP-coated Mg alloy were measured at 0.19 μm , 1.97 μm , and 1.33 μm , respectively (Fig. 4a, c). The surface contact angles of bare Mg alloy, MAO pre-treated Mg alloy, and CMP-coated Mg alloy were 108°, 105°, and 65°, respectively (Fig. 4b). The average thickness of the MgO layer made by MAO pre-treatment layer was 20.6 \pm 0.8 μm . After being coated with CMP, the coating layer was significantly enhanced to 22.6 \pm 0.3 μm (Fig. 4d). The thickness of the coating layer may be controlled by adjusting the processing parameters of MAO pre-treatment (e.g. voltage value, current values, and processing time) [33] as well as the number of repeated sol-gel treatments [34]. The stereo microscope images showed that the

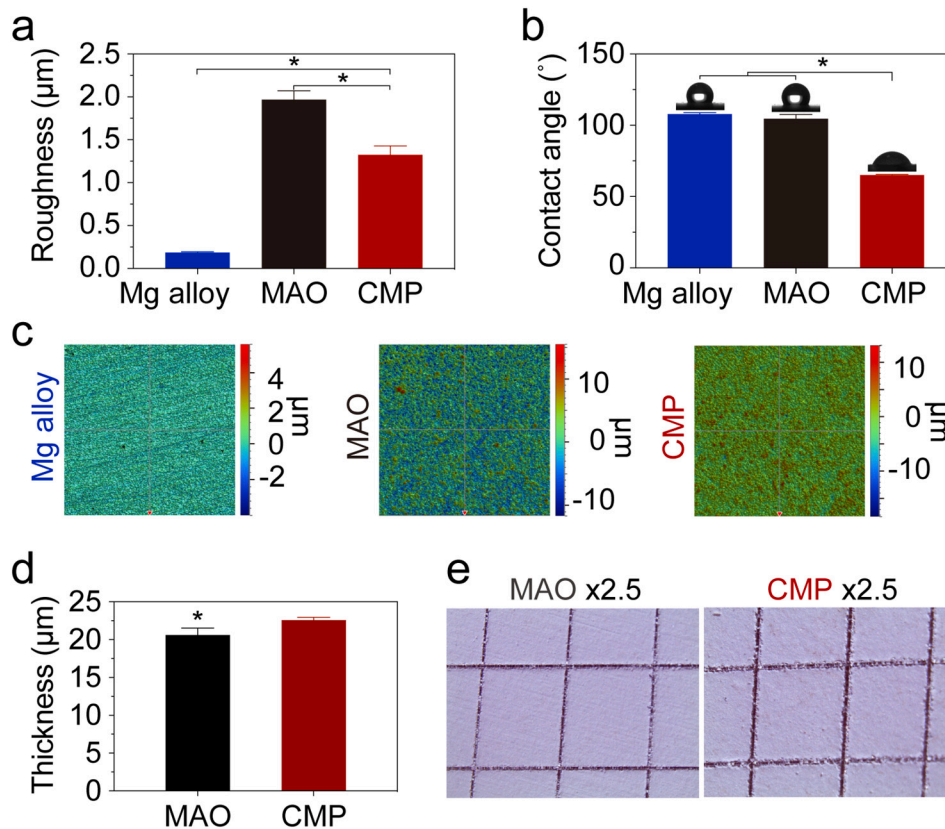


Fig. 4. Material Characterization. (a) Surface roughness in Ra measured by profilometer, and (c) the representative images of surface morphology. (b) Surface wettability measured by the water contact angle test, and the representative images of water droplets. (d) The thickness of the MAO pretreated coating and that of the CMP coating. (e) Stereo microscopic images after performing the cross-cut test. Error bars represent one standard deviation (* $p < 0.05$).

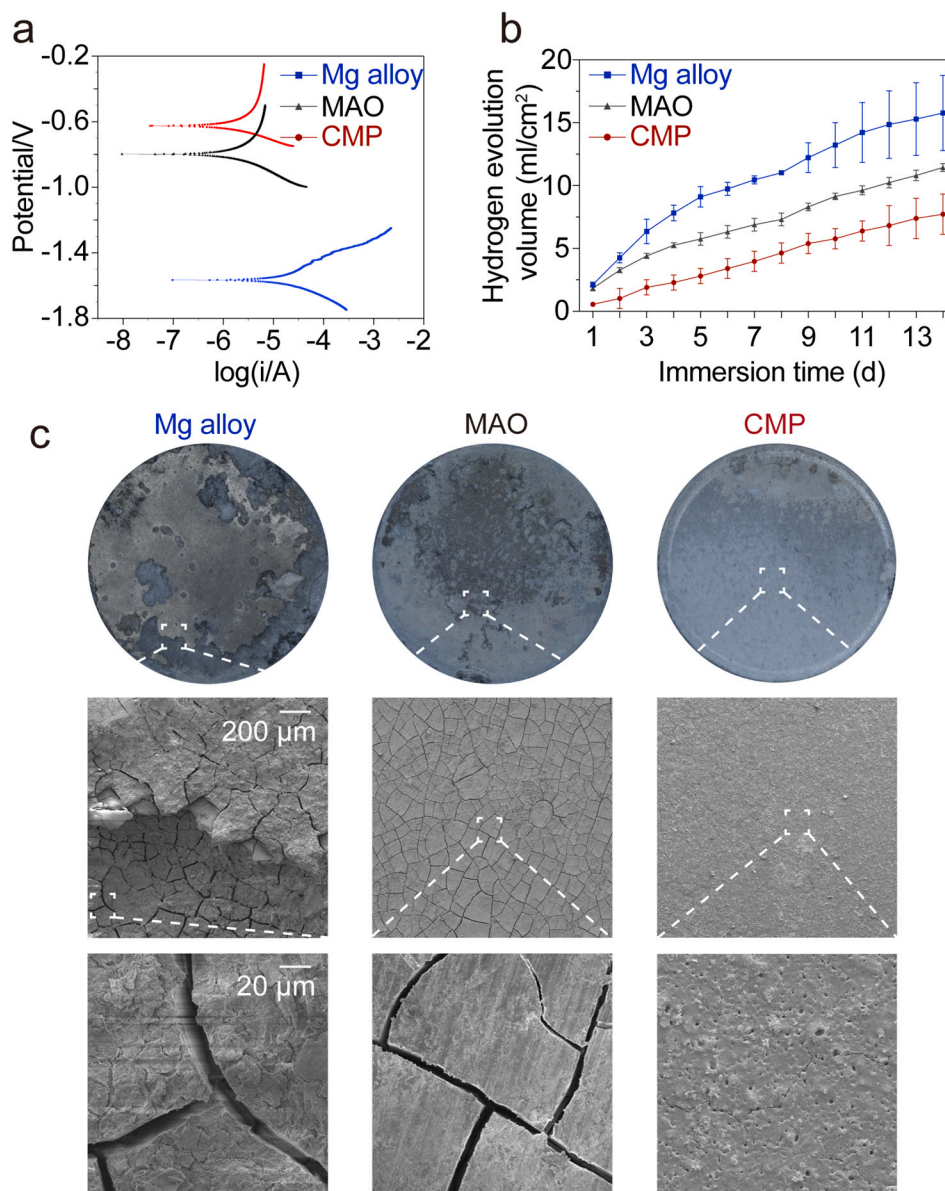


Fig. 5. Corrosion behavior. (a) Tafel polarization curves. (b) Hydrogen evolution volumes as a function of immersion time for 14 days in simulated body fluid. (c) Samples corrosion morphology after immersed for 14 days were presented by digital camera and scanning electron microscope.

edges of cuts on MAO pre-treated Mg alloy and CMP coated Mg alloy were both smooth (Fig. 4e) and none of the lattice was detached (classification 0), indicating that the MAO pre-treated layer and CMP coating were both firmly attached to the Mg alloy substrate. This high adhesion strength of sol-gel CMP coating assisted with MAO pre-treatment may result from to the insertion of coating into the MAO layer [26,35]. The porous MAO pre-treatment layer locked with the sol-gel CMP coating due to the enhanced contact area between coating and substrate [26]. Moreover, the heat treatment in present study also partially contributes to the strong bonding of CMP coating [36].

3.2. Corrosion resistance behavior

The corresponding polarization curves of bare Mg alloy substrates, MAO pre-treated Mg alloy, and CMP-coated Mg alloy are shown in Fig. 5a. According to the Tafel extrapolation, compared with that of the bare Mg alloy ($E_{\text{corr}} = -1.565$ V, $i_{\text{corr}} = 1.400 \times 10^{-6}$ A/cm²), the MAO-pretreated Mg alloy increased the E_{corr} value to -0.799 V and reduced the i_{corr} value to 6.527×10^{-8} A/cm². The CMP coated Mg

alloy further increased the E_{corr} value to -0.626 V, and decreased i_{corr} value to 3.775×10^{-8} A/cm². Although the decrease in corrosion current density is not much, this 1–2 order of magnitude of decrease of i_{corr} value agrees with the results of other studies about preparing calcium phosphate coating on Mg or Mg alloys for bone repair application [2,5,30].

To further study the improvement on corrosion resistance behavior of Mg alloy by constructing CMP coating, an immersion test was carried out. From the Eq. (1) that describes the degradation reaction of Mg, and the rate of hydrogen evolution is proportional to the Mg alloy degradation rate. The degradation of CMP coated Mg alloy included three processes. First, the hydrolytic degradation of CMP at the outer layer of the coating began with phosphate since CMP is a polymeric structure consisting of phosphate chains [14]. Second, the inner layer MgO of MAO pre-treated layer degraded according to the reaction described by Eq. (2) [37]. Third, Mg alloy degraded followed Eq. (1)



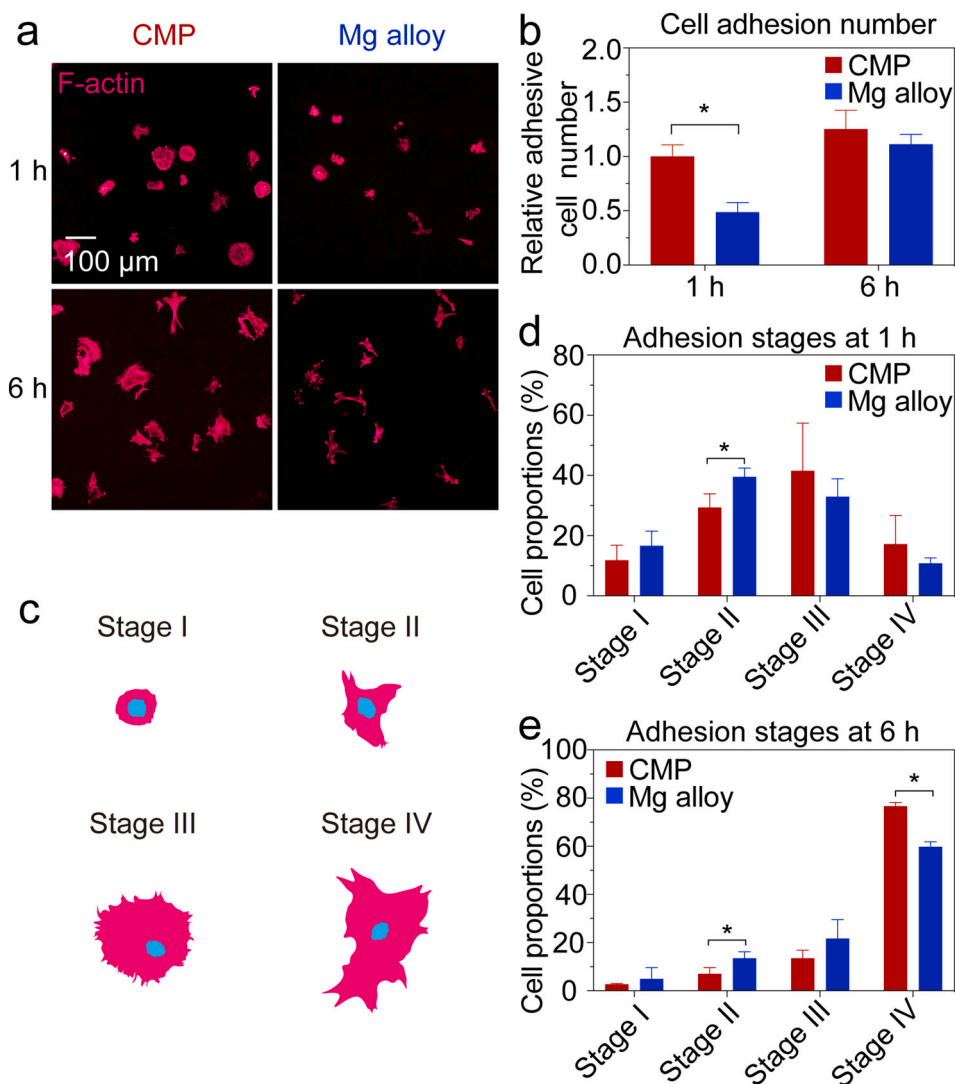
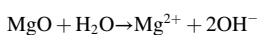


Fig. 6. Cell adhesion. (a) Representative fluorescent images of F-actin (pink, pseudo color) of hBMSCs cultured on CMP coated Mg alloy and bare Mg alloy substrate at 1 h and 6 h. (b) The cell adhesion number at 1 h and 6 h. (c) Schematic diagram of the four stages of cell adhesion morphology. Proportions of cells in each adhesion stage at (d) 1 h and (e) 6 h. Error bars represent one standard deviation (* $p < 0.05$). (For interpretation of the references to color in this figure legend, the reader is referred to the web version of this article.)



With the increase of immersion time, our results showed that the hydrogen evolution volume of CMP coated Mg alloy increased more slowly than that of only MAO pre-treated samples, which also increased more slowly than that of bare Mg alloy substrate (Fig. 5b). The surface morphology of bare Mg alloy substrate, MAO pre-coated Mg alloy, and CMP coated Mg alloy after immersed for 14 days were also presented by digital camera and scanning electron microscope (Fig. 5c). The only MAO pre-treated Mg alloy maintained more integrity as compared to bare Mg alloy substrate. Smaller and fewer corrosion pits, defects and cracks were found on CMP coated Mg alloy than those on the surface of only MAO pre-treated samples. This trend of the immersion results is in accordance to the that of potentiodynamic polarization study discussed above.

As shown by our results in Fig. 5, MAO pre-treatment could significantly reduce the degradation rate of the Mg alloy. This could be attributable to the fact that most part of Mg alloy has been covered by the MgO layer generated by MAO [38], although there are some micro pores as the molten oxide and gas bubbles exited the micro-arc discharge channels [19,38]. This protection effect of MAO layer for Mg and Mg alloy was also reported by other previous study [38]. When CMP sol-gel coating was made, the corrosion rate of Mg alloy was further reduced, which may result from the sealing of the micro pores on the MAO pre-treatment layer (Fig. 1) [40].

3.3. Osteogenic cell behavior

The cell morphology of hBMSCs at attachment phase was displayed by fluorescence images (Fig. 6a). There were significantly more hBMSCs attached on the CMP coated surface than that on the bare Mg alloy surface after the early attachment phase (1 h). There was no significant difference in the attached cell number between the two groups after 6 h (Fig. 6b). The process of cell adhesion can be divided into four stages according their morphological appearance: round cells in stage I, round cells with filopodia in stage II, cells with cytoplasmic webbing in stage III, and flattened cells in stage IV (Fig. 6c) [41]. Most of the hBMSCs on both the CMP coated and bare surfaces entered stages II and III, while more cells on the bare Mg alloy surface entered stage II after 1 h than those on the CMP coated surface (Fig. 6d). After 6 h, almost all cells on the CMP coated surface had entered stage IV (Fig. 6e). These results indicate that CMP coating accelerated the adhesion process of hBMSCs as compared to bare Mg alloy substrate.

After 24 h, hBMSCs completed the process of adhesion and spreading onto the material surfaces. Cell spreading was evaluated by immunostaining of vinculin and F-actin, both playing crucial roles in focal adhesions of cells [42]. The immunostaining images of vinculin (Fig. 7a) and subsequent analysis (Fig. 7b, c) show that the area and number of focal adhesions per cell was significantly larger on CMP coating than that on bare Mg alloy substrate. The immunostaining images of F-actin

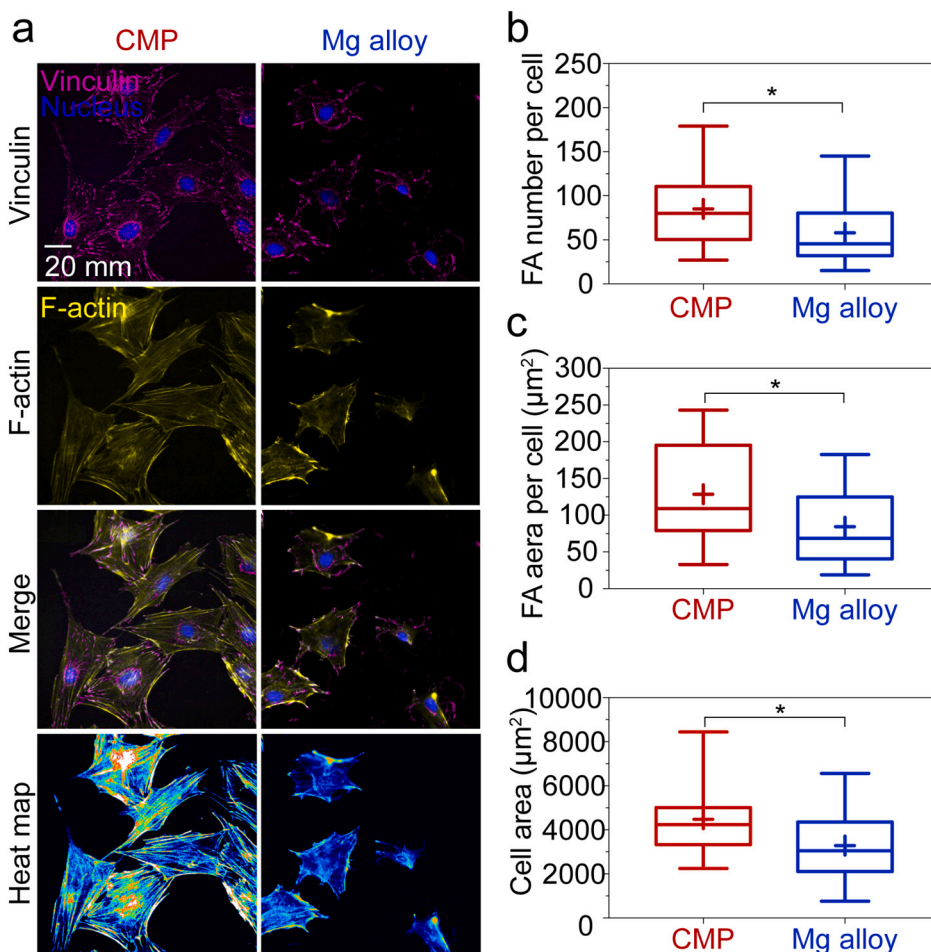


Fig. 7. Cell spreading. (a) Representative fluorescent images of vinculin (purple), nuclei (blue), and F-actin (yellow, pseudo color) of hBMSCs cultured on CMP coated Mg alloy and bare Mg alloy substrate at 24 h. Quantitative analysis of the (b) number and (c) area of focal adhesion (FA) per cell. (d) Quantitative analysis of cell spreading area. Error bars represent one standard deviation ($*p < 0.05$). (For interpretation of the references to color in this figure legend, the reader is referred to the web version of this article.)

(Fig. 7a) and corresponding analysis (Fig. 7d) display that hBMSCs exhibited larger spreading area with more obvious stress fibre formation on CMP coating than on bare Mg alloy substrate. During the degradation progress of the bare Mg alloy substrate, the abundant hydrogen directly caused cell attachment and spreading to decrease [6,43]. CMP coating can delay the degradation progress (Fig. 5). Moreover, the CMP coated surfaces were more conducive to cell adhesion and spreading in the early stage, which can be also partially explained by the hydrophilic properties (Fig. 4b) of the CMP coating [44].

Ki-67 is a nuclear protein that is associated with cellular proliferation, which is present during all active phases of the cell cycle (G1, S, G2, and mitosis) [45]. The results (Fig. 8a, b) show the Ki-67 positive proportion in cells was higher for CMP coating than bare Mg alloy substrate. This indicates that the CMP coating stimulates more hBMSCs to enter the proliferation state [46]. The results are also in agreement with that of the Cell Counting Kit-8 experiment (Fig. 8c), where more hBMSCs were found on CMP coating within the experiment period up to 72 h. This observation can be attributed to the faster cell adhesion, better cell spreading and higher proportion of cells entering the proliferative phase on CMP coating surface as compared with the bare Mg alloy [40].

The osteoinductivity of CMP was estimated from the level of molecular and genetic expression in the cells. The hBMSCs on CMP coated surface were clearly stained blue after ALP staining, whereas little staining was observed in cells on the bare Mg alloy (Fig. 9a). After cultivation for 7 days, the relative *ALP*, *COL1*, and *RUNX2* mRNA expression levels in hBMSCs cultured on the CMP-coated surface were significantly higher than those in cells on bare Mg alloy surface (Fig. 9b–d). Additionally, the Cell Counting Kit-8 and ALP staining were also carried out on only MAO pre-treated surface. The cell proliferation

on MAO pre-treated surface was superior to that on Mg alloy substrate but inferior to that on CMP coating (Fig. S1). However, only very little ALP expression was found on the MAO pre-treated surface as compared to CMP coated samples (Fig. S2). This indicates that the osteoinductivity should be mainly contribute to the CMP coating, whose chemical properties are similar to those of bone [47,48].

Previous studies reported some calcium phosphate coatings prepared on Mg or Mg alloy could delay their degradation rate and provide them osteoinductivity [17,26,49]. It should be noted that without applying an appropriate pre-treatment such as MAO in present study, the coating adhesion is often too weak to meet the clinical requirements [19,26], and the Mg ion released during the coating preparation procedure may inhibit the crystallization of calcium phosphate [20,21]. Moreover, as compared with hydroxyapatite, the most widely-reported coating matrix, previous study has demonstrated that CMP can induce better osteogenic differentiation of hBMSCs [11]. However, how this CMP coating system made on Mg alloy performs as compared with other calcium phosphate coatings in more complex *in vivo* environments needs for further study.

4. Conclusions

CMP coatings were successfully prepared on Mg alloys using MAO pre-treatment assisted sol-gel coating approach. The CMP-coated substrate exhibited a higher corrosion resistance than the bare magnesium alloy. Additionally, the CMP coating facilitated the cell osteogenic behavior of hBMSCs, including cell adhesion, spreading, proliferation, and osteogenic differentiation. These results might inform the further development of surface modifications for Mg alloys in bone related

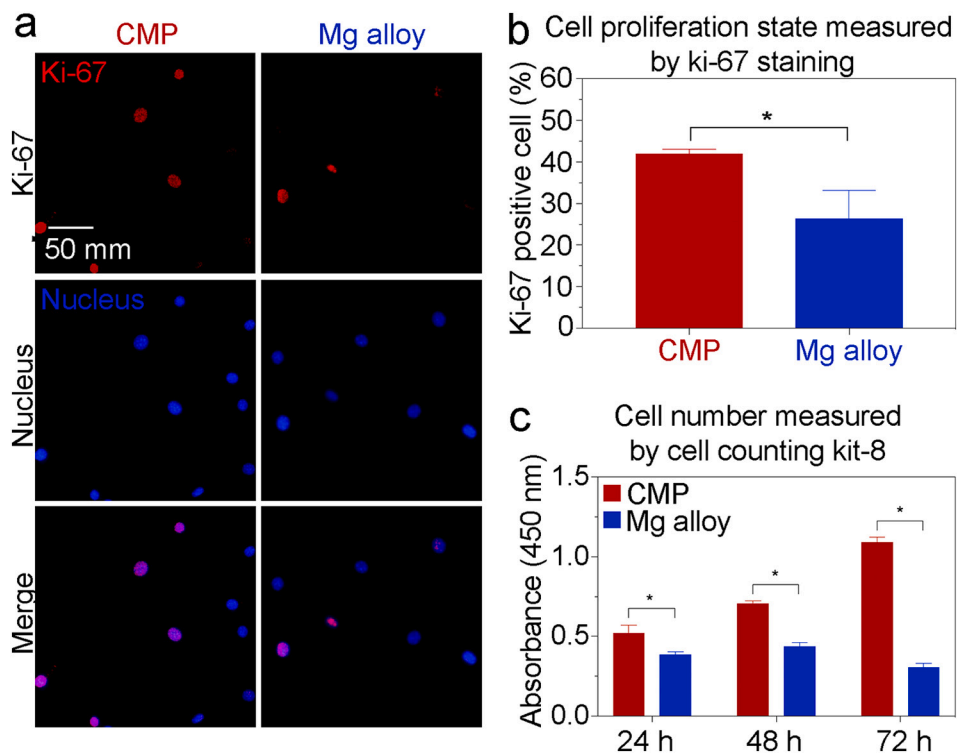


Fig. 8. Cell proliferation. (a) Representative fluorescent images of Ki-67 (red) and nuclei (blue) of hBMSCs on CMP coated Mg alloy and bare Mg alloy substrate at 24 h. (b) Quantitative analysis of Ki-67-positive cells. (c) Cell counting kit-8 assay at 24 h, 48 h, and 72 h. Error bars represent one standard deviation (* $p < 0.05$). (For interpretation of the references to color in this figure legend, the reader is referred to the web version of this article.)

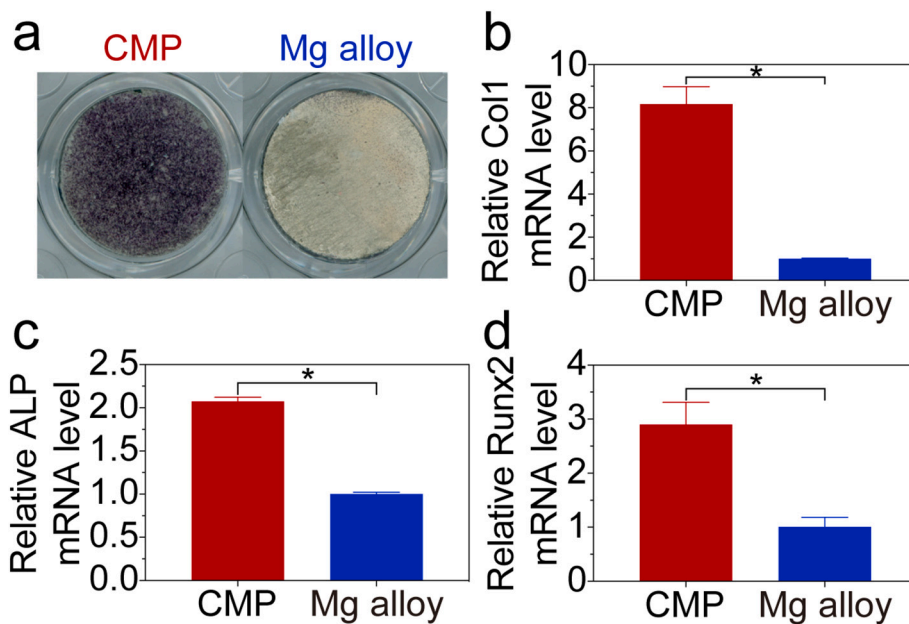


Fig. 9. Osteoblast differentiation. (a) Images of ALP staining hBMSCs cultured on bare and CMP coated Mg alloys at 7 days. Relative mRNA expression levels of (b) ALP, (c) COL1, and (d) RUNX2 at 7 days. Error bars represent one standard deviation (* $p < 0.05$).

applications.

CRediT authorship contribution statement

Y.P.L., X.C., X.Y.W, Q.S., and C.X.W. performed the experiments and analyzed the data. Y.P.L., X.C., and X.Y.W designed the experiments. P. D. and Y.L. supervised the study. Y.P.L., X.C., P.D., and Y.L. have

contributed to writing or revising the manuscript and final approval.

Declaration of competing interest

The authors declare that they have no known competing financial interests or personal relationships that could have appeared to influence the work reported in this paper.

Acknowledgements

The authors thank the National Natural Science Foundation of China (grant number 81771106), and the National Key Research and Development Program of China (grant number 2016YFC1102705).

Appendix A. Supplementary data

Supplementary data to this article can be found online at <https://doi.org/10.1016/j.msec.2021.112491>.

References

- [1] D. Zhao, F. Witte, F. Lu, J. Wang, J. Li, L. Qin, Current status on clinical applications of magnesium-based orthopaedic implants: a review from clinical translational perspective, *Biomaterials* 112 (2017) 287–302.
- [2] J.L. Gao, Y.C. Su, Y.X. Qin, Calcium phosphate coatings enhance biocompatibility and resistance of magnesium alloy: correlating in vitro and in vivo studies, *Bioact. Mater.* 6 (5) (2021) 1223–1229.
- [3] M. Yazdimamaghani, M. Razavi, D. Vashae, K. Moharamzadeh, A.R. Boccaccini, L. Tayebi, Porous magnesium-based scaffolds for tissue engineering, *Mater. Sci. Eng. C Mater. Biol. Appl.* 71 (2017) 1253–1266.
- [4] Y. Chen, Z. Xu, C. Smith, J. Sankar, Recent advances on the development of magnesium alloys for biodegradable implants, *Acta Biomater.* 10 (11) (2014) 4561–4573.
- [5] M.B. Kannan, O. Wallipa, Potentiostatic pulse-deposition of calcium phosphate on magnesium alloy for temporary implant applications—an in vitro corrosion study, *Mater. Sci. Eng. C* 33 (2) (2013) 675–679.
- [6] H. Hornberger, S. Virtanen, A. Boccaccini, Biomedical coatings on magnesium alloys—a review, *Acta Biomater.* 8 (7) (2012) 2442–2455.
- [7] M. Razavi, M. Fath, O. Savabi, S.M. Razavi, B.H. Beni, D. Vashae, L. Tayebi, Controlling the degradation rate of bioactive magnesium implants by electrophoretic deposition of akermanite coating, *Ceram. Int.* 40 (3) (2014) 3865–3872.
- [8] M. Razavi, M. Fathi, O. Savabi, D. Vashae, L. Tayebi, Improvement of biodegradability, bioactivity, mechanical integrity and cytocompatibility behavior of biodegradable mg based orthopedic implants using nanostructured bredigite (Ca₇MgSi₄O₁₆) bioceramic coated via ASD/EPD technique, *Ann. Biomed. Eng.* 42 (12) (2014) 2537–2550.
- [9] P. Makkar, H.J. Kang, A.R. Padalhin, O. Faruq, B. Lee, In-vitro and in-vivo evaluation of strontium doped calcium phosphate coatings on biodegradable magnesium alloy for bone applications, *Appl. Surf. Sci.* (2020) 145333.
- [10] Y. Jung, S.-S. Kim, Y.H. Kim, S.-H. Kim, B.-S. Kim, S. Kim, C.Y. Choi, S.H. Kim, A poly (lactic acid)/calcium metaphosphate composite for bone tissue engineering, *Biomaterials* 26 (32) (2005) 6314–6322.
- [11] E.K. Park, Y.E. Lee, J.Y. Choi, S.H. Oh, H.I. Shin, K.H. Kim, S.Y. Kim, S. Kim, Cellular biocompatibility and stimulatory effects of calcium metaphosphate on osteoblastic differentiation of human bone marrow-derived stromal cells, *Biomaterials* 25 (17) (2004) 3403–3411.
- [12] Y.M. Lee, Y.J. Seol, Y.T. Lim, S. Kim, S.B. Han, I.C. Rhyu, S.H. Baek, S.J. Heo, J. Y. Choi, P.R. Klokkevd, Tissue-engineered growth of bone by marrow cell transplantation using porous calcium metaphosphate matrices 54 (2) (2001) 216–223.
- [13] C. You, I.-S. Yeo, M.-D. Kim, T.-K. Eom, J.-Y. Lee, S. Kim, Characterization and in vivo evaluation of calcium phosphate coated cp-titanium by dip-spin method, *Curr. Appl. Phys.* 5 (5) (2005) 501–506.
- [14] S. Oh, M.-H. Han, W.-B. Im, S.Y. Kim, K.H. Kim, C. You, J.L. Ong, Surface characterization and dissolution study of biodegradable calcium metaphosphate coated by sol-gel method, *J. Sol-Gel Sci. Technol.* 53 (3) (2010) 627–633.
- [15] K. Ishikawa, E. Garskaite, A. Kareiva, Sol-gel synthesis of calcium phosphate-based biomaterials—a review of environmentally benign, simple, and effective synthesis routes 94 (3) (2020) 551–572.
- [16] L. Gan, R. Pilliar, Calcium phosphate sol-gel-derived thin films on porous-surfaced implants for enhanced osteoconductivity. Part I: Synthesis and characterization 25 (22) (2004) 5303–5312.
- [17] Hsieh Ming-Fa, Perng Li-Hsiang, Chin Tsung-Shune, Hydroxyapatite coating on Ti6Al4V alloy using a sol-gel derived precursor, *Mater. Chem. Phys.* 74 (3) (2002) 245–250.
- [18] X.H. Zheng, Q. Liu, H.J. Ma, S. Das, Y.H. Gu, L. Zhang, Probing local corrosion performance of sol-gel/MAO composite coating on mg alloy, *Surf. Coat. Technol.* 347 (2018) 286–296.
- [19] A. Bigi, G. Falini, E. Foresti, A. Ripamonti, M. Gazzano, N. Roveri, Magnesium influence on hydroxyapatite crystallization, *J. Inorg. Biochem.* 49 (1) (1993) 69–78.
- [20] J. Li, Y. Song, S. Zhang, C. Zhao, F. Zhang, X. Zhang, L. Cao, Q. Fan, T. Tang, In vitro responses of human bone marrow stromal cells to a fluoridated hydroxyapatite coated biodegradable Mg–Zn alloy, *Biomaterials* 31 (22) (2010) 5782–5788.
- [21] Z. Yao, L. Li, Z. Jiang, Adjustment of the ratio of Ca/P in the ceramic coating on mg alloy by plasma electrolytic oxidation, *Appl. Surf. Sci.* 255 (13–14) (2009) 6724–6728.
- [22] J. Han, P. Wan, Y. Sun, Z. Liu, X. Fan, L. Tan, K. Yang, Fabrication and evaluation of a bioactive Sr–Ca–P contained micro-arc oxidation coating on magnesium strontium alloy for bone repair application, *J. Mater. Sci. Technol.* 32 (3) (2016) 233–244.
- [23] W. Yang, D. Xu, J. Wang, X. Yao, J. Chen, Microstructure and corrosion resistance of micro arc oxidation plus electrostatic powder spraying composite coating on magnesium alloy, *Corros. Sci.* 136 (2018) 174–179.
- [24] D. Jiang, H. Zhou, S. Wan, G.-Y. Cai, Z.-H. Dong, Fabrication of superhydrophobic coating on magnesium alloy with improved corrosion resistance by combining micro-arc oxidation and cyclic assembly, *Surf. Coat. Technol.* 339 (2018) 155–166.
- [25] B. Niu, P. Shi, E. Shanshan, D.H. Wei, Q. Li, Y. Chen, Preparation and characterization of HA sol-gel coating on MAO coated AZ31 alloy, *Surf. Coat. Technol.* 286 (2016) 42–48.
- [26] X.N. Gu, W. Zheng, Y. Cheng, Y.F. Zheng, A study on alkaline heat treated mg-ca alloy for the control of the biocorrosion rate, *Acta Biomater.* 5 (7) (2009) 2790–2799.
- [27] U. Horzum, B. Ozdil, D. Pesen-Okvur, Step-by-step quantitative analysis of focal adhesions, *MethodsX* 1 (2014) 56–59.
- [28] R.-C. Zeng, L.-Y. Cui, K. Jiang, R. Liu, B.-D. Zhao, Y.-F. Zheng, In vitro corrosion and cytocompatibility of a microarc oxidation coating and poly (l-lactic acid) composite coating on Mg–Li–Ca alloy for orthopedic implants, *ACS Appl. Mater. Interfaces* 8 (15) (2016) 10014–10028.
- [29] S.-Y. Jian, S.L. Aktug, H.-T. Huang, C.-J. Ho, S.-Y. Lin, C.-H. Chen, M.-W. Wang, C.-C. Tseng, The potential of calcium/phosphate containing MAO implanted in bone tissue regeneration and biological characteristics, *Int. J. Mol. Sci.* 22 (9) (2021) 4706.
- [30] A. Jaafar, C. Hecker, P. Árki, Y. Joseph, Sol-gel derived hydroxyapatite coatings for titanium implants: a review, *Bioengineering* 7 (4) (2020) 127.
- [31] K. Ishikawa, E. Garskaite, A. Kareiva, Sol-gel synthesis of calcium phosphate-based biomaterials—a review of environmentally benign, simple, and effective synthesis routes, *J. Sol-Gel Sci. Technol.* 94 (3) (2020) 551–572.
- [32] M.M.S. Al Bosta, K.J. Ma, H.H. Chien, The effect of MAO processing time on surface properties and low temperature infrared emissivity of ceramic coating on aluminium 6061 alloy, *Infrared Phys. Technol.* 60 (2013) 323–334.
- [33] V. Ezhilselvi, J. Nithin, J. Balaraju, S. Subramanian, The influence of current density on the morphology and corrosion properties of MAO coatings on AZ31B magnesium alloy, *Surf. Coat. Technol.* 288 (2016) 221–229.
- [34] J.H. Gao, S.K. Guan, J. Chen, L.G. Wang, S.J. Zhu, J.H. Hu, Z.W. Ren, Fabrication and characterization of rod-like nano-hydroxyapatite on MAO coating supported on Mg–Zn–Ca alloy, *Appl. Surf. Sci.* 257 (6) (2011) 2231–2237.
- [35] S.B. Shen, S. Cai, G.H. Xu, H. Zhao, S.X. Niu, R.Y. Zhang, Influence of heat treatment on bond strength and corrosion resistance of sol-gel derived bioglass-ceramic coatings on magnesium alloy, *J. Mech. Behav. Biomed.* 45 (2015) 166–174.
- [36] Z. Yao, Q. Xia, L. Chang, C. Li, Z. Jiang, Structure and properties of compound coatings on mg alloys by micro-arc oxidation/hydrothermal treatment, *J. Alloys Compd.* 633 (2015) 435–442.
- [37] T.S.N.S. Narayanan, I.S. Park, M.H. Lee, Strategies to improve the corrosion resistance of microarc oxidation (MAO) coated magnesium alloys for degradable implants: prospects and challenges, *Prog. Mater. Sci.* 60 (2014) 1–71.
- [38] H. Tang, W. Tao, C. Wang, H. Yu, Fabrication of hydroxyapatite coatings on AZ31 mg alloy by micro-arc oxidation coupled with sol-gel treatment, *RSC Adv.* 8 (22) (2018) 12368–12375.
- [39] Y. Long, X. Cheng, J.A. Jansen, S.G.C. Leeuwenburgh, J. Mao, F. Yang, L. Chen, The molecular conformation of silk fibroin regulates osteogenic cell behavior by modulating the stability of the adsorbed protein-material interface, *Bone Res.* 9 (1) (2021) 1–12.
- [40] X. Cheng, D. Long, L. Chen, J.A. Jansen, S.G.C. Leeuwenburgh, F. Yang, Electrophoretic deposition of silk fibroin coatings with pre-defined architecture to facilitate precise control over drug delivery, *Bioactive materials* 6 (11) (2021) 4243–4254.
- [41] X. Cheng, D. Deng, L. Chen, J.A. Jansen, S.G.C. Leeuwenburgh, F. Yang, Electrodeposited assembly of additive-free silk fibroin coating from pre-assembled nanospheres for drug delivery, *ACS Appl. Mater. Interfaces* 12 (10) (2020) 12018–12029.
- [42] L. Wistlich, J. Kums, A. Rossi, K.H. Heffels, H. Wajant, J. Groll, Multimodal bioactivation of hydrophilic electrospun nanofibers enables simultaneous tuning of cell adhesivity and immunomodulatory effects, *Adv. Funct. Mater.* 27 (46) (2017) 1702903.
- [43] X. Cheng, F. Yang, More than just a barrier—challenges in the development of guided bone regeneration membranes, *Matter* 1 (3) (2019) 558–560.
- [44] D. Long, X. Cheng, Z. Hao, J. Sun, D. Umuhzoza, Y. Liu, L. Chen, Z. Xiang, F. Yang, A. Zhao, Genetic hybridization of highly active exogenous functional proteins into silk-based materials using “light-clothing” strategy, *Matter* 4 (6) (2021) 2039–2058.
- [45] J.M. Sadowska, F. Wei, J. Guo, J. Guillem-Marti, Z. Lin, M.-P. Ginebra, Y. Xiao, The effect of biomimetic calcium deficient hydroxyapatite and sintered β-tricalcium phosphate on osteoimmune reaction and osteogenesis, *Acta Biomater.* 96 (2019) 605–618.
- [46] M. Bohner, R.J. Miron, A proposed mechanism for material-induced heterotopic ossification, *Mater. Today* 22 (2019) 132–141.
- [47] H. Tang, T.Z. Xin, F.P. Wang, Calcium Phosphate/Titania sol-gel coatings on AZ31 magnesium alloy for biomedical applications, *Int. J. Electrochem. Sci.* 8 (6) (2013) 8115–8125.